JCI insight

Hydroxysteroid 17-β dehydrogenase 13 variant increases phospholipids and protects against fibrosis in nonalcoholic fatty liver disease

Panu K. Luukkonen, … , Matej Orešič, Hannele Yki-Järvinen

JCI Insight. 2020;5(5):e132158. https://doi.org/10.1172/jci.insight.132158.

Research Article | Hepatology | Metabolism

Carriers of the hydroxysteroid 17-β dehydrogenase 13 (HSD17B13) gene variant (rs72613567:TA) have a reduced risk of NASH and cirrhosis but not steatosis. We determined its effect on liver histology, lipidome, and transcriptome using ultra performance liquid chromatography-mass spectrometry and RNA-seq. In carriers and noncarriers of the gene variant, we also measured pathways of hepatic fatty acids (de novo lipogenesis [DNL] and adipose tissue lipolysis [ATL] using $^{2}H_2O$ and ^{2}H-glycerol) and insulin sensitivity using ^{3}H-glucose and euglycemic-hyperinsulinemic clamp) and plasma cytokines. Carriers and noncarriers had similar age, sex and BMI. Fibrosis was significantly less frequent while phospholipids, but not other lipids, were enriched in the liver in carriers compared with noncarriers. Expression of 274 genes was altered in carriers compared with noncarriers, consisting predominantly of downregulated inflammation-related gene sets. Plasma IL-6 concentrations were lower, but DNL, ATL and hepatic insulin sensitivity were similar between the groups. In conclusion, carriers of the HSD17B13 variant have decreased fibrosis and expression of inflammation-related genes but increased phospholipids in the liver. These changes are not secondary to steatosis, DNL, ATL, or hepatic insulin sensitivity. The increase in phospholipids and decrease in fibrosis are opposite to features of choline-deficient models of liver disease and suggest HSD17B13 as an attractive therapeutic target.

JCI insight

RESEARCH ARTICLE

Hydroxysteroid 17-β dehydrogenase 13 variant increases phospholipids and protects against fibrosis in nonalcoholic fatty liver disease

Panu K. Luukkonen,[1,2,3] Taru Tukiainen,[4] Anne Juuti,[5] Henna Sammalkorpi,[5] P.A. Nidhina Haridas,[2] Onni Niemelä,[6] Johanna Arola,[7] Marju Orho-Melander,[8] Antti Hakkarainen,[9,10] Petri T. Kovanen,[11] Om Dwivedi,[4] Leif Groop,[4,8] Leanne Hodson,[12] Amalia Gastaldelli,[13] Tuulia Hyötyläinen,[14] Matej Orešič,[15,16] and Hannele Yki-Järvinen[1,2]

[1]Department of Medicine, University of Helsinki and Helsinki University Hospital, Helsinki, Finland. [2]Minerva Foundation Institute for Medical Research, Helsinki, Finland. [3]Yale School of Medicine, Yale University, New Haven, Connecticut, USA. [4]Institute for Molecular Medicine Finland, Helsinki, Finland. [5]Department of Surgery, University of Helsinki and Helsinki University Hospital, Helsinki, Finland. [6]Department of Laboratory Medicine and Medical Research Unit, Seinäjoki Central Hospital and University of Tampere, Tampere, Finland. [7]Department of Pathology, University of Helsinki and Helsinki University Hospital, Helsinki, Finland. [8]Department of Clinical Sciences, Lund University, Malmö, Sweden. [9]Department of Radiology, HUS Medical Imaging Center, Helsinki University Hospital and University of Helsinki, Helsinki, Finland. [10]Department of Neuroscience and Biomedical Engineering, Aalto University School of Science, Espoo, Finland. [11]Wihuri Research Institute, Helsinki, Finland. [12]Oxford Centre for Diabetes, Endocrinology and Metabolism, University of Oxford, Oxford, United Kingdom. [13]Institute of Clinical Physiology, Consiglio Nazionale delle Ricerche, Pisa, Italy. [14]Department of Chemistry, Örebro University, Örebro, Sweden. [15]Turku Centre for Biotechnology, University of Turku and Åbo Akademi University, Turku, Finland. [16]School of Medical Sciences, Örebro University, Örebro, Sweden.

Carriers of the hydroxysteroid 17-β dehydrogenase 13 (HSD17B13) gene variant (rs72613567:TA) have a reduced risk of NASH and cirrhosis but not steatosis. We determined its effect on liver histology, lipidome, and transcriptome using ultra performance liquid chromatography-mass spectrometry and RNA-seq. In carriers and noncarriers of the gene variant, we also measured pathways of hepatic fatty acids (de novo lipogenesis [DNL] and adipose tissue lipolysis [ATL] using $^{2}H_{2}O$ and ^{2}H-glycerol) and insulin sensitivity using ^{3}H-glucose and euglycemic-hyperinsulinemic clamp) and plasma cytokines. Carriers and noncarriers had similar age, sex and BMI. Fibrosis was significantly less frequent while phospholipids, but not other lipids, were enriched in the liver in carriers compared with noncarriers. Expression of 274 genes was altered in carriers compared with noncarriers, consisting predominantly of downregulated inflammation-related gene sets. Plasma IL-6 concentrations were lower, but DNL, ATL and hepatic insulin sensitivity were similar between the groups. In conclusion, carriers of the HSD17B13 variant have decreased fibrosis and expression of inflammation-related genes but increased phospholipids in the liver. These changes are not secondary to steatosis, DNL, ATL, or hepatic insulin sensitivity. The increase in phospholipids and decrease in fibrosis are opposite to features of choline-deficient models of liver disease and suggest HSD17B13 as an attractive therapeutic target.

Conflict of interest: The authors have declared that no conflict of interest exists.

Submitted: July 29, 2019
Accepted: February 5, 2020
Published: March 12, 2020.

Reference information: *JCI Insight*. 2020;5(5):e132158. https://doi.org/10.1172/jci.insight.132158.

Introduction

A protein-truncating variant (rs72613567:TA), encoding the hepatic lipid droplet protein hydroxysteroid 17-β dehydrogenase 13 (HSD17B13), was recently reported to reduce risks of alcoholic and nonalcoholic cirrhosis (1, 2), fibrosis (1–3), and histologic signs of inflammation and ballooning (3). The variant does not seem protective against steatosis (1–3). The mechanism(s) via which the variant confers protection to liver disease are unclear.

Until now, 15 17β-hydroxysteroid dehydrogenases (HSD17Bs) have been identified in humans. HSD17B1–HSD17B6 regulate sex steroid metabolism, while others are involved in regulation of fatty and bile acid metabolism and cholesterol biosynthesis (4, 5). HSD17B13 is a lipid droplet–associated

protein (3, 6), mainly expressed in the liver (7). It is a target gene for the insulin-regulated lipogenic transcription factor steroid responsive element–binding protein 1c (SREBP1c) (8) and upregulated in the liver in human nonalcoholic fatty liver disease (NAFLD) (6). This could be secondary to hyperinsulinemia and increased de novo lipogenesis (DNL) in NAFLD associated with insulin resistance (9) or a consequence of HSD17B13, because overexpression of this protein caused steatosis in mice and increased lipid droplet size and number in cultured human hepatocytes (6). Mouse data are, however, contradictory as knockout of HSD17B13 induced steatosis in male mice (10). Furthermore, in a recent study neither stable overexpression nor silencing of *HSD17B13* altered lipogenesis in HepG2 cells (2). Intracellular triglyceride content was unaltered in oleic acid treated cell lines overexpressing HSD17B13 isoforms A and D, i.e., the transcripts encoding full-length (predominant in reference allele homozygotes [T/T]) and prematurely truncated (predominant in alternate allele homozygotes [TA/TA]) proteins (1). Whether the gene variant alters pathways contributing fatty acids to intrahepatic triglycerides (IHTG) in humans has not been investigated.

HSD17B3 has enzymatic activity against several lipid substrates that have been implicated in lipid-mediated inflammation, including metabolites originating from phospholipids (1). Each of the recently described major genetic variants increasing the risk of NAFLD fibrosis influence metabolism of hepatic phospholipids. Patatin-like phospholipase domain–containing protein 3 (PNPLA3) functions in fatty acid remodeling by transferring polyunsaturated fatty acid from triglycerides to phospholipids (11). Loss of this function results in accumulation of polyunsaturated fatty acids in triglycerides in the mouse liver (11) and the human liver of carriers of the PNPLA3 I148M gene variant (12). Impaired incorporation of polyunsaturated fatty acids into hepatic triglycerides, phospholipids, and cholesterol esters characterizes transmembrane 6 superfamily member 2 (TM6SF2) E167K variant carriers with NAFLD (13). Membrane-bound O-acyltransferase domain containing 7 (MBOAT7) is a lysophosphatidylinositol acyltransferase, which catalyzes acyl-chain remodeling of phosphatidylinositols and alters plasma and liver phosphatidylinositol concentrations (14, 15).

In the present study, we wished to characterize the human liver lipidome and transcriptome in carriers and noncarriers of the *HSD17B13* variant (rs72613567:TA). Furthermore, as there are no data on whether the HSD17B13 variant influences the major pathways contributing fatty acids to IHTG synthesis in humans or insulin sensitivity, we quantified DNL using deuterated water, insulin sensitivity using the euglycemic insulin clamp technique, and rates of basal and insulin-stimulated lipolysis using deuterated glycerol in carriers and noncarriers of the *HSD17B13* variant.

Results

Characteristics of the study groups

Clinical characteristics of the HSD17B13 genotype groups with liver histology data are shown in Table 1. The groups were similar with respect to age, sex, and BMI (Table 1). The TTA/TATA group had lower aspartate aminotransferase (AST) (29.5 ± 1.2 vs. 36.7 ± 2.6 IU/L, $P < 0.05$, Table 1) compared with the TT group. Concentrations of fasting glucose, insulin, and lipids in the circulation as well as distributions of PNPLA3, TM6SF2, and MBOAT7 genotypes were comparable among the HSD17B13 genotype groups (Table 1).

Liver histology. Macrovesicular steatosis and necroinflammatory activity were similar between the groups (Figure 1 and Table 1). The prevalence of fibrosis was significantly lower in the TTA/TATA group as compared with the TT group (25.0% vs. 42.4%, $P < 0.05$, Figure 1 and Table 1). There were no subjects with significant fibrosis (fibrosis stage ≥2) in the TTA/TATA group as compared with the 6.8% of the subjects with significant fibrosis in the TT group ($P < 0.05$, Table 1).

Clinical characteristics of the subjects in whom pathways of hepatic triglyceride synthesis and insulin sensitivity were measured are shown in Supplemental Tables 1–5 (supplemental material available online with this article; https://doi.org/10.1172/jci.insight.132158DS1).

Lipidomic analysis

The $\log_2$ fold changes in liver lipids in the TTA/TATA group as compared with the TT group are shown in Figure 2. Among all lipids, exclusively phospholipids were significantly altered. Specifically, concentrations of phosphatidylcholines (PCs), such as PC(p16:0/16:0), PC(44:5e), PC(36:2e), and PC(34:3), and phosphatidylethanolamines (PEs), such as PE(p16:0/18:1), PE(34:0) and PE(36:3), were increased in the liver

Table 1. Clinical characteristics of the study subjects with liver histology data grouped by the HSD17B13 genotype at rs72613567

	TT (*n* = 118)	TTA/TATA (*n* = 84)
Age (yr)	46.1 ± 0.8	47.0 ± 1.0
Sex (% women)	80.5	76.2
BMI (kg/m^2)	41.5 ± 0.7	42.1 ± 0.8
Waist circumference (cm)	121.1 ± 1.5	122.6 ± 1.8
fP-Glucose (mmol/L)	5.5 (5.1–5.9)	5.6 (5.2–5.8)
HbA_{1c} (%)	5.5 (5.2–5.7)	5.6 (5.4–5.8)
HbA_{1c} (mmol/mol)	36.6 (33.3–41.0)	37.7 (35.5–39.9)
fS-Insulin (mU/L)	11.2 (6.9–17.4)	11.1 (7.7–16.2)
HOMA-IR	2.9 (1.7–4.5)	2.9 (1.8–4.1)
fP-Triglycerides (mmol/L)	1.09 (0.82–1.45)	1.11 (0.85–1.63)
fP-HDL cholesterol (mmol/L)	1.17 (1.02–1.49)	1.21 (0.99–1.48)
fP-LDL cholesterol (mmol/L)	2.7 ± 0.1	2.9 ± 0.1
P-AST (IU/L)	36.7 ± 2.6	29.5 ± 1.2[A]
P-ALT (IU/L)	44.4 ± 4.2	37.8 ± 3.2
P-ALP (IU/L)	73.4 ± 3.8	77.0 ± 4.7
P-GGT (IU/L)	50.2 ± 7.3	44.3 ± 4.9
P-Albumin (g/L)	38.7 ± 0.3	38.3 ± 0.3
B-Platelets (×10^9/L)	250 ± 5	255 ± 7
Macrovesicular steatosis (%)	5 (0–20)	5 (0–20)
Steatosis score (%, 0/1/2/3)	50/38/6/7	43/45/8/4
Activity grade (%, 0/1/2/3/4)	93/4/4/0/0	93/5/3/0/0
Ballooning (%, 0/1/2)	96/4/0	95/5/0
Inflammation (%, 0/1/2)	93/7/0	95/5/0
Fibrosis stage (%, 0/1/2/3/4)	58/35/6/0/1	75/25/0/0/0[A]
HSD17B13 genotype (%,TT/TTA/TATA)	100/0/0	0/90/10[A]
PNPLA3 genotype (%, CC/CG/GG)	58/34/7	54/40/6
TM6SF2 genotype (%, CC/CT/TT)	86/13/1	91/8/1
MBOAT7 genotype (%, CC/CT/TT)	37/51/12	33/47/20

Data are shown as percentage and mean ± SEM or median (25th–75th percentile), as appropriate. [A]$P \le 0.05$. fP, fasting plasma; fS, fasting serum; P, plasma; B, blood.

in the TTA/TATA group as compared with the TT group (Figure 2). The increases in individual liver PC species in the TTA/TATA versus the TT group were virtually uniform and did not depend on the number of double bonds or carbons in a given species (Supplemental Figure 1, A and B). In liver PEs, the greatest increases in the TTA/TATA versus the TT group were in species with 0–4 double bonds and 32–40 carbons (Supplemental Figure 1, C and D).

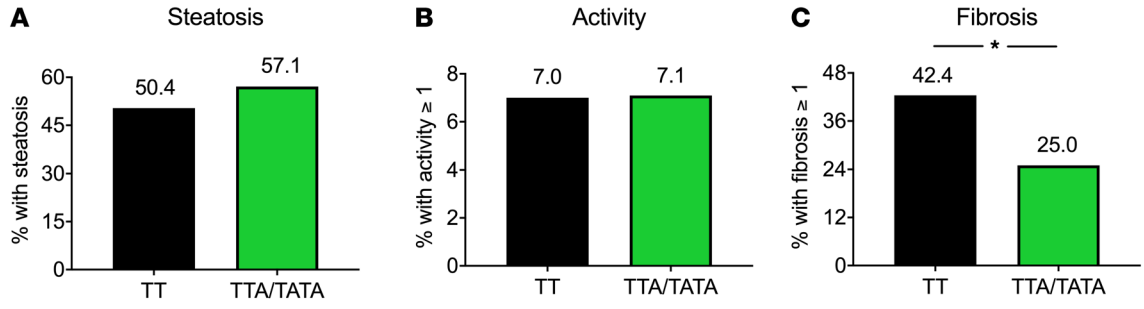

Figure 1. Decreased hepatic fibrosis in carriers of the HSD17B13 rs72613567 variant. (**A**) The percentage of subjects with steatosis (macrovesicular steatosis, ≥5%). (**B**) The percentage of subjects with necroinflammatory activity (activity grade, ≥1). (**C**) The percentage of subjects with fibrosis (fibrosis stage, ≥1) in the TT (*n* = 118) and TTA/TATA (*n* = 84) groups, as determined histologically using the SAF score. Distributions were tested using Pearson's χ^2 test. Black bars = TT; green bars = TTA/TATA. *$P < 0.05$.

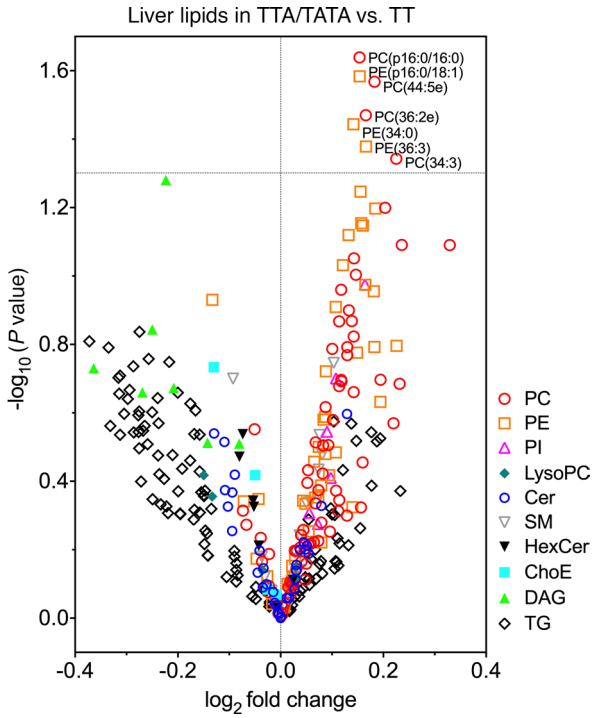

Figure 2. Increased hepatic phospholipids in carriers of the HSD17B13 rs72613567 variant. Liver lipids are visualized as a volcano plot, in which *y* axes denote the $-\log_{10}$ of *P* value of the *t* test between individual lipid species in the TTA/TATA (n = 38) as compared with the TT group (n = 48) and *x* axes denote the $\log_2$ fold change of mean concentrations of an individual lipid species between the HSD17B13 groups. Differences were tested using independent 2-sample Student's *t* test. Each symbol denotes an individual lipid species. PC, phosphatidylcholine; PE, phosphatidylethanolamine; PI, phosphatidylinositol; LysoPC, lyso-phosphatidylcholine; Cer, ceramide; SM, sphingomyelin; HexCer, hexosylceramide; ChoE, cholesteryl ester; DAG, diacylglycerol; TG, triacylglycerol.

Hepatic transcriptome

In hepatic transcriptome analysis, a total of 274 genes were differentially expressed ($q < 0.05$) in the TTA/TATA group as compared with the TT group (Figure 3A). Among these 274 genes, 166 were downregulated (Supplemental Table 6) and 108 were upregulated (Supplemental Table 7).

Individual genes that were differentially expressed in the TTA/TATA group as compared with the TT group were analyzed using gene set enrichment analysis of gene ontology (GO) pathways. A total of 254 gene sets were downregulated (Supplemental Table 8) and 2 pathways were upregulated in the TTA/TATA group as compared with the TT group (Supplemental Table 9). The top 20 most significantly downregulated gene sets in the TTA/TATA group as compared with the TT group are visualized as an enrichment map in Figure 3B. These include several inflammation-related gene sets, such as Activation of immune response ($q < 2.16 \times 10^{-6}$), Positive regulation of innate immune response ($q < 4.66 \times 10^{-6}$), Activation of innate immune response ($q < 1.61 \times 10^{-5}$), and Positive regulation of defense response ($q < 3.90 \times 10^{-5}$) (Figure 3B). Downregulated genes that were enriched in these gene sets include arachidonate 5-lipoxygenase (*ALOX5*), hypoxia-inducible factor 1 subunit α (*HIF1A*) and TGF-β2 (*TGFB2*) (Supplemental Figure 2). Upregulated genes in the TTA/TATA group as compared with the TT group included lipin 3 (*LPIN3*) (Supplemental Table 7).

RNA-seq was followed by quantitative PCR (qPCR) analyses, in which downregulation of *ALOX5* (0.77 ± 0.04 vs. 1.00 ± 0.06 AU, $P < 0.01$) and *TGFB2* (0.79 ± 0.05 vs. 1.00 ± 0.06 AU, $P < 0.01$) and upregulation of *LPIN3* (1.23 ± 0.10 vs. 1.00 ± 0.04 AU, $P < 0.05$) were confirmed (Figure 3C). Among genes involved in phospholipid metabolism, the expression of phospholipase family member D4 (*PLD4*) was significantly decreased (0.83 ± 0.06 vs. 1.00 ± 0.06 AU, $P < 0.05$) in TTA/TATA group as compared with the TT group (Figure 3C).

Plasma cytokines

Since the gene expression profile suggested that carriers of the HSD17B13 variant might be characterized by decreased inflammation, we measured plasma concentrations of cytokines (Figure 3D). Plasma concentrations of IL-6 were significantly lower in the TTA/TATA group as compared with the TT group (9.0 ± 0.5 vs. 10.2 ± 0.5 pg/ml, $P < 0.05$) (Figure 3D).

Liver free fatty acids and their sources

Hepatic fatty acids are the major substrates for synthesis of complex lipids, such as triacylglycerols and phospholipids. They can be derived from the diet, adipose tissue lipolysis, and hepatic DNL (16). There were no

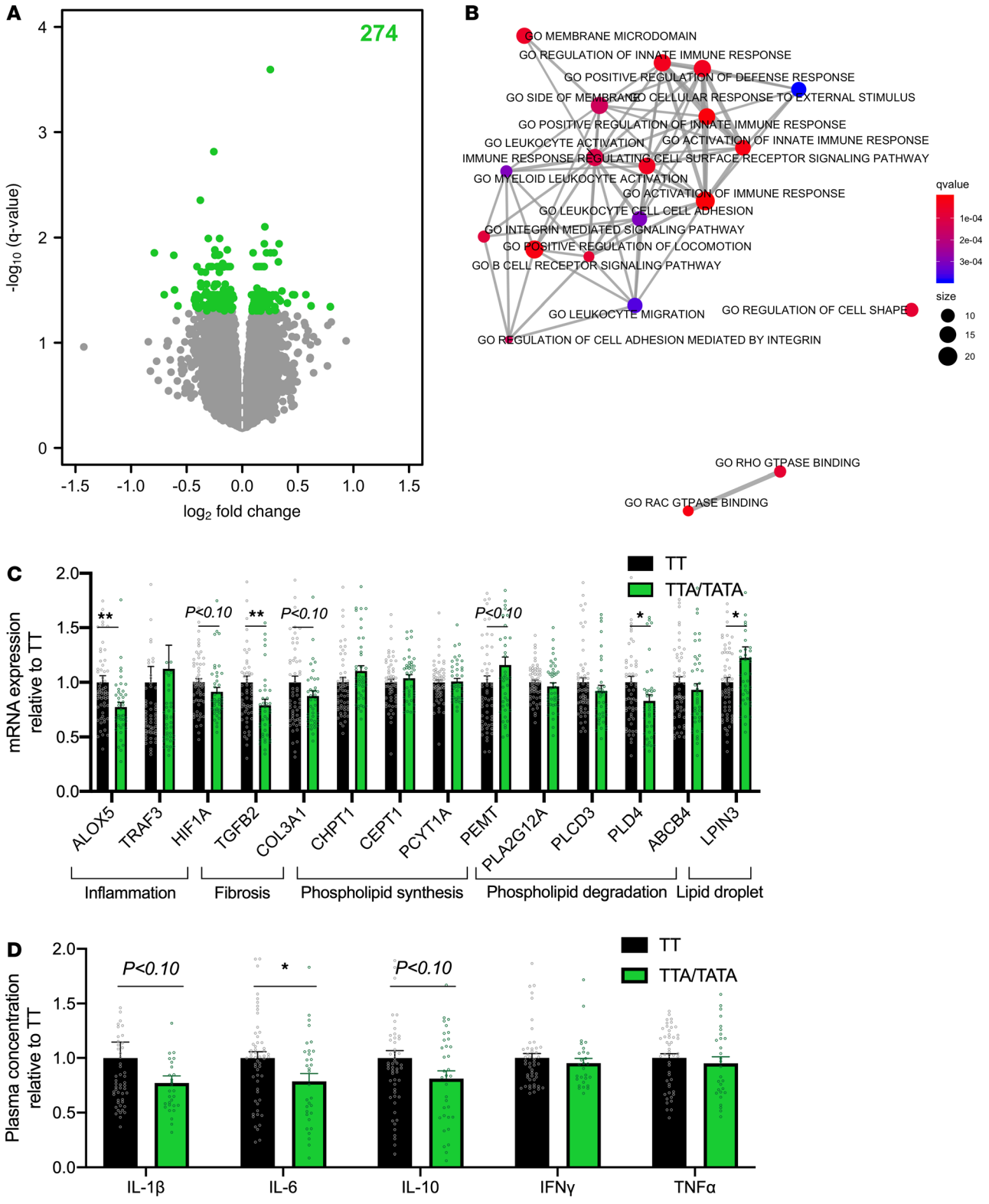

Figure 3. Decreased hepatic inflammation in carriers of the HSD17B13 rs72613567 variant. (**A**) Volcano plot of differentially expressed genes in the livers of carriers (TTA/TATA, *n* = 36) as compared with noncarriers (TT, *n* = 50) of the HSD17B13 rs72613567 variant. The *x* axes denote $\log_2$ fold change and *y* axes denote the $-\log_{10}$ of the q value of expression of genes in the livers of carriers as compared with noncarriers. The number in green denotes the amount of significantly differentially expressed genes. The analysis was performed by limma. (**B**) Enrichment map of gene ontology (GO) pathways of differentially expressed genes in the livers of carriers as compared with noncarriers of the HSD17B13 variant. Data were analyzed using the enricher function in the clusterProfiler R package. The color of the bubbles denotes q values and size denotes the number of genes in the pathway. (**C**) Quantitative PCR analysis of hepatic gene expression in the TTA/TATA (green bars and circles, *n* = 42) groups as compared with the TT group (black bars and circles, *n* = 60). The

data were tested using independent 2-sample Student's *t* test and are expressed relative to the TT group as mean ± SEM. *$P < 0.05$. ALOX5, arachidonate 5-lipoxygenase; TRAF3, TNF receptor–associated factor 3; HIF1A, hypoxia-inducible factor 1 subunit α; TGFB2, TGF-β2; COL3A1, collagen type III α 1 chain; CHPT1, choline phosphotransferase 1; CEPT1, choline/ethanolamine phosphotransferase 1; PCYT1A, phosphate cytidylyltransferase 1; PEMT, phosphatidylethanolamine N-methyltransferase; PLA2G12A, phospholipase A2, group XIIA; PLCD3, phospholipase C δ 3; PLD4, phospholipase D family member 4; ABCB4, ATP binding cassette subfamily B member 4; LPIN3, lipin 3. (**D**) Plasma concentrations of IL-1β, IL-6, IL-10, IFN-γ, and TNF-α in the TTA/TATA (green bars and circles, $n = 45$) groups as compared with the TT group (black bars and circles, $n = 70$). The data were analyzed using independent 2-sample Student's *t* test and are expressed relative to the TT group as mean ± SEM. *$P < 0.05$.

differences in free fatty acids (398 ± 17 vs. 382 ± 12 nmol/g for 16:0, 219 ± 11 vs. 195 ± 7 nmol/g for 18:0, 196 ± 9 vs. 194 ± 8 nmol/g for 18:1, 86 ± 4 vs. 89 ± 4 nmol/g for 18:2 and 54 ± 3 vs. 54 ± 2 nmol/g for 20:4, respectively, NS) in the liver in the TTA/TATA group as compared with the TT group (Figure 4). The rate of adipose tissue lipolysis, as determined by the rate of appearance (R_a) of glycerol, was similar between the HSD17B13 groups both in the basal state (2.92 ± 0.24 vs. 3.12 ± 0.16 μmol/kg.min, NS, Figure 4) and during euglycemic hyperinsulinemia (1.66 ± 0.19 vs. 1.63 ± 0.09 μmol/kg.min, NS, Figure 4). The rate of hepatic DNL, as determined by the percentage of newly synthesized palmitate in VLDL-triglyceride, was comparable in the TTA/TATA and the TT groups (7.5 ± 0.8 vs. 7.7 ± 0.8%, NS, Figure 4).

Hepatic glucose production and insulin sensitivity

The hepatic glucose production (R_a of glucose) was similar in the basal state (2.82 ± 0.13 vs. 3.08 ± 0.14 mg/kg FFM.min, Figure 4) and during euglycemic hyperinsulinemia (0.65 ± 0.20 vs. 0.74 ± 0.18 mg/kg FFM.min, Figure 4) in the TTA/TATA group as compared with the TT group.

Discussion

We found lower prevalence of fibrosis (Figure 1 and Table 1) and increased concentration of phospholipids in the livers of subjects carrying the *HSD17B13* rs72613567:TA variant compared with noncarriers (Figure 2). Analysis of the liver transcriptome using RNA-seq and qPCR revealed marked downregulation of multiple inflammation-related gene sets (Figure 3). Plasma concentrations of the key proinflammatory cytokine, IL-6, were lower in carriers of the HSD17B13 variant as compared with noncarriers (Figure 3). Metabolic pathways contributing to IHTG synthesis, including DNL and the rate of in vivo lipolysis and hepatic insulin sensitivity, were unaltered in carriers of the *HSD17B13* variant compared with noncarriers (Figure 4).

The prevalence of fibrosis, the most important predictor of mortality in NAFLD (17), was significantly lower in carriers compared with noncarriers of the HSD17B13 variant (Figure 1 and Table 1), consistent with the study of Abul-Husn et al. (1) and that of Pirola et al. in 356 patients with biopsy-proven NAFLD (3). In the latter 2 studies, as in the present study, the HSD17B13 variant was not associated with a change in steatosis (Figure 1) (1, 3). In a larger study comprising 756 adults with biopsy-proven NAFLD, Ma et al. found increased steatosis in carriers compared with noncarriers of the *HSD17B13* variant (rs72613567:TA) (2). Unlike previous studies, features of nonalcoholic steatohepatitis (NASH) were similar in our data (Figure 1 and Table 1). This could reflect a smaller sample size compared with previous studies.

Concentrations of hepatic phospholipids, including PCs and PEs, but not other lipids including triglycerides, DAGs, or ceramides, were increased in variant allele carriers compared with noncarriers (Figure 2). This lipid pattern is geometrically opposite to that seen in deficiency of choline, an essential nutrient, in which concentrations of PCs and PEs are decreased (18, 19). Dietary restriction of choline predisposes to fatty liver in humans, and its daily requirements to prevent liver dysfunction are highly variable (18, 20, 21). In mice, dietary restriction of choline and/or genetic inhibition of hepatic PC synthesis lead to liver inflammation, NASH (22), and liver failure (23). In contrast, increasing PC synthesis by choline treatment has been shown to prevent both sugar- and alcohol-induced cirrhosis in rats in carefully performed studies published in 1949 (24). Moreover, dietary supplementation of PC has been shown to protect against alcohol-induced liver fibrosis and cirrhosis in nonhuman primates, possibly by promoting collagen breakdown (25). Decreased expression of a phospholipid degrading enzyme *PLD4* (Figure 3C) suggests that the phospholipid surplus could be secondary to the reduced degradation of phospholipids in HSD17B13 variant carriers as compared with noncarriers. Phospholipids constitute the surface layer of lipid droplets, and their excess could be hypothesized to enhance storage capacity of lipid droplets, in keeping with increased hepatic expression of a key lipid droplet protein, LPIN3, in HSD17B13 variant carriers (Figure 3C). The present data thus raise the possibility that the HSD17B13 variant might protect against progressive liver disease, perhaps especially

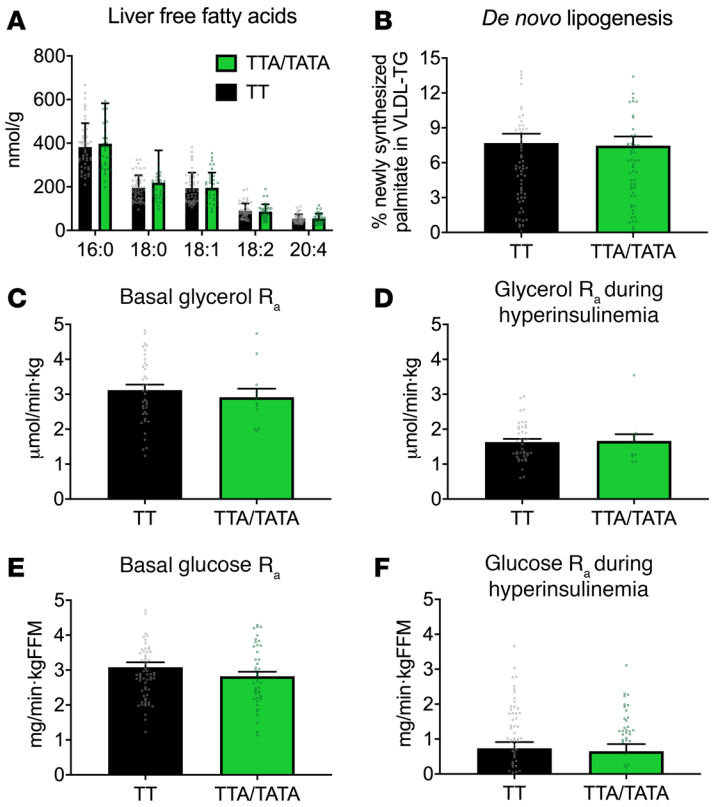

Figure 4. Hepatic free fatty acids, de novo lipogenesis, adipose tissue lipolysis, and hepatic insulin sensitivity are similar in carriers and noncarriers of the HSD17B13 rs72613567 variant. (**A**) The concentrations of individual hepatic free fatty acids (TT, *n* = 48; TTA/TATA, *n* = 38) and (**B**) the rate of hepatic de novo lipogenesis (TT, *n* = 67; TTA/TATA, *n* = 59) in the HSD17B13 groups. (**C**) The rate of appearances of glycerol in the basal state and (**D**) during euglycemic hyperinsulinemia in the TT (*n* = 40) and TTA/TATA (*n* = 12) groups. (**E**) The rate of appearances of glucose in the basal state and (**F**) during euglycemic hyperinsulinemia in the TT (*n* = 62) and TTA/TATA (*n* = 43) groups. The data were analyzed using independent 2-sample Student's *t* test and are shown as mean ± SEM. Black bars = TT; green bars = TTA/TATA. FFM, fat free mass.

in choline-depleted individuals, by increasing synthesis and/or decreasing breakdown of hepatic phospholipids. The molecular mechanisms linking phospholipids and progression of fibrosis are poorly understood, but at least in choline- and methionine-depleted models include altered redox status and inflammation (26). While these findings are of interest, given the extensive literature on altered choline metabolism and liver disease (18–25), they do not prove cause and effect and call for further mechanistic studies.

Analysis of the liver transcriptome in 86 subjects using RNA-seq revealed downregulation of 254 gene sets while only 2 gene sets were upregulated in carriers compared with noncarriers (Figure 3). The downregulated genes were predominantly key inflammatory genes, such as ALOX5 and TGFB2. In keeping with the gene expression data, plasma concentrations of IL-6, a proinflammatory cytokine that has increased concentrations in NASH (27), were decreased in carriers of the HSD17B13 variant as compared with noncarriers (Figure 3D). These data are consistent with previous data on effects of the *HSD17B13* variant on the liver transcriptome in the study of Pirola et al. who compared 8 carriers to 5 noncarriers (3).

Free fatty acids originating from lipolysis and DNL are two major pathways contributing to IHTG synthesis (16). Although steatosis was not different in the present study or studies by Abul-Husn et al. (1) or Pirola et al (3), pathways of IHTG could still be different, as has been described for the PNPLA3 I148M gene variant (28). However, the *HSD17B13* variant does not seem to alter either DNL or adipose tissue lipolysis when measured using state-of-the-art isotope techniques, including deuterated water and glycerol.

Unlike NAFLD associated with the PNPLA3 I148M and the TM6SF2 E167K gene variants, common NAFLD is characterized by insulin resistance (29). This is the first study to our knowledge to quantify insulin sensitivity using the euglycemic clamp technique combined with infusion of tritiated glucose between

HSD17B13 variant allele carriers and noncarriers. No data on glucose and insulin concentrations were reported in studies by Abul-Husn et al. (1) or Ma et al. (2). Unlike the latter studies, in the study of Pirola et al. (3), homozygous variant allele carriers were significantly less obese than the heterozygous subjects or noncarriers (3). We found that the *HSD17B13* variant allele did not affect any measure of insulin sensitivity. If viewed from the perspective of the effect of choline deficiency on insulin sensitivity, previous studies in mice fed a choline-deficient diet, which induces steatosis and mild inflammation, showed that mice do not exhibit insulin resistance (30). Thus, the higher concentrations of PCs and PEs in carriers than noncarriers of the *HSD17B13* variant would not be expected to change insulin sensitivity.

We conclude that carriers of the *HSD17B13* variant are protected against liver fibrosis and that they have phospholipid surplus in the liver and marked downregulation of genes and plasma cytokines related to inflammation. Steatosis and pathways leading to steatosis, including DNL and lipolysis, are unchanged. All of these features are geometrically opposite to those observed in choline-deficient models in mice and humans and suggest that HSD17B13 might be an attractive pharmaceutical target in liver disease.

Methods

Study subjects

Histology and lipid composition of the human liver. A total of 485 subjects was included in the study, of which 202 subjects were recruited from patients undergoing laparoscopic bariatric surgery. Subjects were eligible if they, after a phone interview and a separate clinical study visit (see below), met the following inclusion criteria: (a) age 18–75 years; (b) no known acute or chronic disease except for features of the metabolic syndrome based on medical history, physical examination, and standard laboratory tests (complete blood count, serum creatinine, electrolyte concentrations); (c) alcohol consumption of less than 20 g per day in women and less than 30 g per day in men; (d) no clinical or biochemical evidence of other liver disease than NAFLD or clinical signs or symptoms of inborn errors of metabolism; and (e) no use of drugs or toxins influencing liver steatosis. Subjects with diabetes were excluded from this cohort, as we wished to study the effect of the *HSD17B13* genotype at rs72613567 rather than that of insulin resistance/diabetes and antidiabetic drugs on the human liver lipid metabolism.

Pathways of hepatic triglyceride synthesis and insulin sensitivity. 283 subjects who were not undergoing bariatric surgery were studied to compare rates of adipose tissue lipolysis, hepatic DNL and hepatic glucose production basally and during hyperinsulinemia using the same inclusion and exclusion criteria as described above.

All subjects were divided into groups based on their HSD17B13 genotype at rs72613567 (carriers of splice variant with adenine insertion, TTA/TATA, and noncarriers, TT).

Study designs

All subjects were invited to a clinical visit for metabolic characterization after an overnight fast. After anthropometric measurements (body weight, height, and waist circumference), an intravenous cannula was inserted in an antecubital vein. Blood was collected for measurement of total blood counts, glycosylated hemoglobin (HbA_{1c}), serum insulin, plasma glucose, LDL and HDL cholesterol, triglyceride, alanine aminotransferase (ALT), AST, alkaline phosphatase (ALP), γ-glutamyltransferase (GGT), and albumin concentrations and for genotyping of PNPLA3 rs738409, TM6SF2 rs58542926, MBOAT7 rs641738, and HSD17B13 rs72613567 as previously described (12–14). Genotype data were in Hardy-Weinberg equilibrium. Serum carbohydrate-deficient transferrin (CDT) and GGT-CDT combination were determined as biomarkers of alcohol consumption using previously established protocols (31).

Histology, transcriptome, and lipid composition of the human liver. The patients undergoing bariatric surgery underwent the metabolic study 1 week prior to surgery, during which the liver biopsy was taken (see below). The body weight of these subjects did not differ between the time of the metabolic study and surgery (129.6 ± 2.0 kg and 129.3 ± 2.2 kg, NS).

Pathways of hepatic triglyceride synthesis and insulin sensitivity. The subjects in whom rates of pathways contributing to IHTG synthesis and hepatic insulin sensitivity were measured participated in a visit at the metabolic study unit and in an imaging visit for measurement of IHTG using proton magnetic resonance spectroscopy (see below) in addition to the metabolic characterization visit.

Liver biopsy and liver histology

Routine wedge biopsy of the liver was taken in the beginning of the surgery. Part of the biopsy was sent to an experienced liver pathologist for analysis of liver histology in a blinded fashion according to the SAF score (32), and, if available, another part was snap-frozen in liquid nitrogen for subsequent analysis of molecular lipids and transcriptome (see below).

Hepatic lipidomic and free fatty acid analysis

Hepatic lipidomic analyses were performed using a Q-TOF Premier (Waters) quadrupole time-of-flight mass spectrometer combined with an Acquity Ultra Performance LC (Waters) liquid chromatography, as described in the Supplemental Methods. Hepatic free fatty acids were analyzed using an Agilent 6890 gas chromatograph equipped with a split/splitless injector (Agilent Technologies), cryogenic dual-stage modulator, and time-of-flight mass spectrometer (Leco Corp.) as described previously (12).

Hepatic transcriptome

Hepatic transcriptome was assessed using RNA-seq (Supplemental Table 11). The samples were prepared using the Illumina TruSeq RNA Sample preparation kit (Illumina), and sequencing was performed using a paired-end 101-bp protocol on the HiSeq2000 platform (Illumina) as described previously (13). The output reads were aligned to human reference genome (GRCh38) using STAR (v2.4.1a), and uniquely mapped fragments were counted against genomic features defined by the Gencode v22 annotation using FeatureCounts software as described previously (13). The data are included in the Supplemental Methods.

mRNA expression of different genes was analyzed by qPCR. RNA from liver tissue biopsies was isolated using the RNeasy Mini Kit (Qiagen). cDNA synthesis was performed using the SuperScript VILO reverse transcriptase kit (Invitrogen) according to the manufacturer's protocol. qPCR was carried out with the LightCycler 480 SYBR Green I Master (Roche) and gene-specific primers (Supplemental Table 10). Relative gene expression was calculated from the Cp (second derivative method) values. Data were normalized to the geometric mean of house keeping controls, β-actin, and acidic ribosomal phosphoprotein P0, 36B4.

Plasma cytokines

Concentrations of plasma IL-1β, IL-6, IL-10, IFN-γ, and TNF-α were measured by Q-Plex Human Cytokine P1 6-Plex ELISA assay (Quansys Biosciences) according to the manufacturer's instructions.

IHTGs

IHTG content was measured by proton magnetic resonance spectroscopy (^{1}H-MRS) using 1.5T Siemens Avanto^{fit} and jMRUI v5.2 software with an AMARES algorithm as described previously (33).

Hepatic DNL

Fasting hepatic DNL was measured from incorporation of deuterium of $^{2}H_2O$ in plasma water (Finnigan GasBench-II, Thermo Fisher Scientific) into palmitate in VLDL-triglyceride using gas chromatography/mass spectrometry with monitoring ions with mass-to-charge ratios (m/z) of 270 (M+0) and 271 (M+1) (34). VLDL was isolated by ultracentrifugation as described previously (33).

Adipose tissue lipolysis

The rate of whole-body lipolysis (rate of appearance [R_a] of glycerol) and effect of insulin on lipolysis were determined by infusing [$^{2}H_5$]glycerol for 120 minutes before (0–120 min) and for 120 minutes during euglycemic hyperinsulinemia maintained using the euglycemic hyperinsulinemic clamp technique as previously described (35). The duration of the insulin infusion was 120 minutes (120–240 min), and rate of the continuous insulin infusion was 0.4 mU/kg per minute (36). The low insulin infusion rate was chosen to optimize the conditions for detecting changes in lipolysis, which is half-maximally suppressed already at insulin concentrations of 13 mU/L in normal subjects (37). The concentrations needed to inhibit hepatic glucose production or stimulate glucose disposal in normal subjects are approximately 50 mU/L and approximately 100 mU/L (38). Before start of the infusions, two 18-gauge catheters (Venflon, Viggo-Spectramed) were inserted, one in a left antecubital vein and another retrogradely in a heated (+65 °C) dorsal hand vein for sampling of arterialized venous blood for insulin (0, 120, 180, and 240 min) and concentrations of glycerol and its isotopic enrichment (0, 100, 120, 130, 140, 150, 180, and 240 min).

Hepatic glucose production and insulin sensitivity

Hepatic glucose production (R_a of glucose) and insulin sensitivity of glucose R_a were assessed by using the euglycemic hyperinsulinemic clamp technique combined with infusion of [3-^{3}H]glucose as described previously (39). Because glucose R_a is more sensitive to suppression by insulin than stimulation of muscle glucose uptake (38), we chose a low insulin infusion rate (0.3 mU/kg per minute) to accurately quantify interindividual variation in hepatic insulin sensitivity. Glucose R_a were calculated using Steele's non–steady-state equations (40).

Statistics

The Kolmogorov-Smirnov test was used to test the normality of continuous variables. The independent 2-sample 2-tailed Student's *t* test and Mann-Whitney *U* test were used to compare normally and nonnormally distributed data, respectively. Normally distributed data were reported in mean ± SEM, while nonnormally distributed data were reported as medians followed by interquartile ranges. Pearson's χ^2 test was used to evaluate if the distribution of categorical variables differed between the groups.

For the lipidomics analyses, data were $\log_2$ transformed and the mean values were compared between groups based on HSD17B13 genotype using unpaired 2-tailed *t* tests. Lipidomics data were visualized using a volcano plot, in which the *y* axes denote the $-\log_{10}$ transformed *P* values and the *x* axes denote the $\log_2$ fold changes in individual lipid concentrations in the TTA/TATA group as compared with the TT group.

Differential expression analyses were conducted to investigate the hepatic transcriptome changes between the HSD17B13 variant allele carriers and noncarriers. Prior to differential expression analyses, normalization factors were calculated from the raw read counts using trimmed mean of M values (TMM) normalization (41) to account for library size variation between samples, and only genes with sufficiently large read counts, i.e., minimum count in at least 1 sample = 10 and minimum total count across samples = 15, were retained, and both procedures were implemented in the edgeR R package (42). To remove unwanted noise from the gene expression data, unknown and unmeasured artifacts were estimated using svaseq (43) with read counts as input and modeling the gene variant, sex, and age as known variables. The association between gene expression and each gene variant was examined using the limma approach to RNA-seq data (44, 45) using read counts adjusted with precision weights from voom (44) in linear modeling (lmFit function) with sex, age, and surrogate variables from the above svaseq step as covariates and applying the empirical Bayes smoothing to standard errors (eBayes function) (46). Q values were estimated from the *P* values separately for each gene variant analysis using the q value R package (ref. 47; http://github.com/jdstorey/qvalue), and $q < 0.05$ was used as the threshold for calling a gene differentially expressed. The gene set enrichment analysis was conducted using the enricher function in the clusterProfiler R package (48) using the differentially expressed genes as the input and analyzing the enrichments for upregulated and downregulated genes separately. The results were visualized using the emapplot and heat plot functions in the enrichplot R package (ref. 49; https://github.com/GuangchuangYu/enrichplot). Gene sets with $q < 0.05$ were considered significantly enriched. The GO gene sets used in the enrichment analyses were obtained from the Molecular Signatures Database (MSigDB) using the msigdbr function (https://CRAN.R-project.org/package=msigdbr). All differential expression and gene set enrichment analyses were conducted in R (version 3.5.2). Other statistical analyses were performed by using IBM SPSS Statistics 22.0.0.0 version, Microsoft Excel 2016, and GraphPad Prism 7.0 for Mac OS X. A 2-sided *P* value of less than 0.05 indicated statistical significance.

Study approval

The studies were reviewed and approved by the ethics committee of the Hospital District of Helsinki and Uusimaa (Helsinki, Finland) and conducted in accordance with the Declaration of Helsinki. Each participant provided written informed consent after the nature and potential risks of the study were fully explained prior to their participation in the study.

Author contributions

PKL conceived and designed the study; performed clinical studies; acquired, analyzed, and interpreted data; and drafted and provided critical revision of the manuscript. TT performed statistical analysis and provided critical revision of the manuscript. AJ, HS, PANH, ON, JA, MOM, AH, OD, LG, LH, AG, TH, and MO acquired data and provided critical revision of the manuscript. PTK interpreted data and provided critical revision of the manuscript. HYJ conceived and designed the study; analyzed and interpreted data; drafted and provided critical revision of the manuscript; and provided study supervision.

Acknowledgments

The authors acknowledge Anne Salo, Aila Karioja-Kallio, Päivi Ihamuotila, and Pentti Pölönen (Helsinki University Hospital) as well as Catriona Charlton and Thomas Cornfield (University of Oxford) for skillful technical assistance and Siiri Luukkonen (University of Oulu) for graphical assistance. This study was supported by grants from the Elucidating Pathways of Steatohepatitis consortium, funded by the Horizon 2020 Framework Program of the European Union under grant agreement 634413 (to HYJ, AG, TH, and MO), and Liver Investigation: Testing Marker Utility in Steatohepatitis, funded by the Innovative Medicines Initiative 2 Joint Undertaking (grant agreement 777377; to HYJ, MO, TH, and AG). The Joint Undertaking receives support from the European Union's Horizon 2020 research and innovation programme and the European Federation of Pharmaceutical Industries and Associations. The study was also supported by grants from the Academy of Finland (to HYJ and TT), EVO (to HYJ), and the Sigrid Juselius (to HYJ and PKL) and Novo Nordisk (to PKL) foundations. AG received grants from the Ministry of Education, Universities and Research and Consiglio Nazionale delle Ricerche, LH holds a British Heart Foundation Senior Fellowship in Basic Science (FS/15/56/31645), and PKL received funds from the Jalmari and Rauha Ahokas and Paulo Foundations. The Wihuri Research Institute is maintained by the Jenny and Antti Wihuri Foundation.

Address correspondence to: Panu K. Luukkonen, Yale School of Medicine, 1 Gilbert Street, New Haven, Connecticut 06519, USA. Phone: 475.300.8865; Email: panu.luukkonen@yale.edu.

1. Abul-Husn NS, et al. A protein-truncating HSD17B13 variant and protection from chronic liver disease. *N Engl J Med*. 2018;378(12):1096–1106.
2. Ma Y, et al. 17-Beta Hydroxysteroid dehydrogenase 13 is a hepatic retinol dehydrogenase associated with histological features of nonalcoholic fatty liver disease. *Hepatology*. 2019;69(4):1504–1519.
3. Pirola CJ, et al. Splice variant rs72613567 prevents worst histologic outcomes in patients with nonalcoholic fatty liver disease. *J Lipid Res*. 2019;60(1):176–185.
4. Saloniemi T, Jokela H, Strauss L, Pakarinen P, Poutanen M. The diversity of sex steroid action: novel functions of hydroxysteroid (17β) dehydrogenases as revealed by genetically modified mouse models. *J Endocrinol*. 2012;212(1):27–40.
5. Su W, et al. Role of HSD17B13 in the liver physiology and pathophysiology. *Mol Cell Endocrinol*. 2019;489:119–125.
6. Su W, et al. Comparative proteomic study reveals 17β-HSD13 as a pathogenic protein in nonalcoholic fatty liver disease. *Proc Natl Acad Sci USA*. 2014;111(31):11437–11442.
7. Horiguchi Y, Araki M, Motojima K. 17beta-Hydroxysteroid dehydrogenase type 13 is a liver-specific lipid droplet-associated protein. *Biochem Biophys Res Commun*. 2008;370(2):235–238.
8. Su W, et al. Liver X receptor α induces 17β-hydroxysteroid dehydrogenase-13 expression through SREBP-1c. *Am J Physiol Endocrinol Metab*. 2017;312(4):E357–E367.
9. Lambert JE, Ramos-Roman MA, Browning JD, Parks EJ. Increased de novo lipogenesis is a distinct characteristic of individuals with nonalcoholic fatty liver disease. *Gastroenterology*. 2014;146(3):726–735.
10. Adam M, et al. Hydroxysteroid (17β) dehydrogenase 13 deficiency triggers hepatic steatosis and inflammation in mice. *FASEB J*. 2018;32(6):3434–3447.
11. Mitsche MA, Hobbs HH, Cohen JC. Patatin-like phospholipase domain–containing protein 3 promotes transfer of essential fatty acids from triglycerides to phospholipids in hepatic lipid droplets. *J Biol Chem*. 2018;293(18):6958–6968.
12. Luukkonen PK, et al. Hepatic ceramides dissociate steatosis and insulin resistance in patients with non-alcoholic fatty liver disease. *J Hepatol*. 2016;64(5):1167–1175.
13. Luukkonen PK, et al. Impaired hepatic lipid synthesis from polyunsaturated fatty acids in TM6SF2 E167K variant carriers with NAFLD. *J Hepatol*. 2017;67(1):128–136.
14. Luukkonen PK, et al. The MBOAT7 variant rs641738 alters hepatic phosphatidylinositols and increases severity of non-alcoholic fatty liver disease in humans. *J Hepatol*. 2016;65(6):1263–1265.
15. Mancina RM, et al. The MBOAT7-TMC4 variant rs641738 increases risk of nonalcoholic fatty liver disease in individuals of European descent. *Gastroenterology*. 2016;150(5):1219–1230.e6.
16. Donnelly KL, Smith CI, Schwarzenberg SJ, Jessurun J, Boldt MD, Parks EJ. Sources of fatty acids stored in liver and secreted via lipoproteins in patients with nonalcoholic fatty liver disease. *J Clin Invest*. 2005;115(5):1343–1351.
17. Dulai PS, et al. Increased risk of mortality by fibrosis stage in nonalcoholic fatty liver disease: Systematic review and meta-analysis. *Hepatology*. 2017;65(5):1557–1565.
18. Zeisel SH, et al. Choline, an essential nutrient for humans. *FASEB J*. 1991;5(7):2093–2098.
19. Corbin KD, Zeisel SH. Choline metabolism provides novel insights into nonalcoholic fatty liver disease and its progression. *Curr Opin Gastroenterol*. 2012;28(2):159–165.
20. Fischer LM, et al. Sex and menopausal status influence human dietary requirements for the nutrient choline. *Am J Clin Nutr*. 2007;85(5):1275–1285.
21. Sha W, et al. Metabolomic profiling can predict which humans will develop liver dysfunction when deprived of dietary choline. *FASEB J*. 2010;24(8):2962–2975.
22. Li Z, et al. The ratio of phosphatidylcholine to phosphatidylethanolamine influences membrane integrity and steatohepatitis. *Cell Metab*. 2006;3(5):321–331.
23. Li Z, Agellon LB, Vance DE. Phosphatidylcholine homeostasis and liver failure. *J Biol Chem*. 2005;280(45):37798–37802.

24. Best CH, Hartroft WS. Liver damage produced by feeding alcohol or sugar and its prevention by choline. *Br Med J*. 1949;2(4635):1002–1006.
25. Lieber CS, et al. Phosphatidylcholine protects against fibrosis and cirrhosis in the baboon. *Gastroenterology*. 1994;106(1):152–159.
26. Serviddio G, et al. Alterations of hepatic ATP homeostasis and respiratory chain during development of non-alcoholic steatohepatitis in a rodent model. *Eur J Clin Invest*. 2008;38(4):245–252.
27. Wieckowska A, Papouchado BG, Li Z, Lopez R, Zein NN, Feldstein AE. Increased hepatic and circulating interleukin-6 levels in human nonalcoholic steatohepatitis. *Am J Gastroenterol*. 2008;103(6):1372–1379.
28. Mancina RM, et al. Paradoxical dissociation between hepatic fat content and de novo lipogenesis due to PNPLA3 sequence variant. *J Clin Endocrinol Metab*. 2015;100(5):E821–E825.
29. Yki-Järvinen H. Non-alcoholic fatty liver disease as a cause and a consequence of metabolic syndrome. *Lancet Diabetes Endocrinol*. 2014;2(11):901–910.
30. Rinella ME, Green RM. The methionine-choline deficient dietary model of steatohepatitis does not exhibit insulin resistance. *J Hepatol*. 2004;40(1):47–51.
31. Niemelä O, et al. Assays of gamma-glutamyl transferase and carbohydrate-deficient transferrin combination from maternal serum improve the detection of prenatal alcohol exposure. *Alcohol Clin Exp Res*. 2016;40(11):2385–2393.
32. Bedossa P, et al. Histopathological algorithm and scoring system for evaluation of liver lesions in morbidly obese patients. *Hepatology*. 2012;56(5):1751–1759.
33. Luukkonen PK, et al. Saturated fat is more metabolically harmful for the human liver than unsaturated fat or simple sugars. *Diabetes Care*. 2018;41(8):1732–1739.
34. Semple RK, et al. Postreceptor insulin resistance contributes to human dyslipidemia and hepatic steatosis. *J Clin Invest*. 2009;119(2):315–322.
35. Yki-Järvinen H, Puhakainen I, Saloranta C, Groop L, Taskinen MR. Demonstration of a novel feedback mechanism between FFA oxidation from intracellular and intravascular sources. *Am J Physiol*. 1991;260(5 Pt 1):E680–E689.
36. DeFronzo RA, Tobin JD, Andres R. Glucose clamp technique: a method for quantifying insulin secretion and resistance. *Am J Physiol*. 1979;237(3):E214–E223.
37. Nurjhan N, Campbell PJ, Kennedy FP, Miles JM, Gerich JE. Insulin dose-response characteristics for suppression of glycerol release and conversion to glucose in humans. *Diabetes*. 1986;35(12):1326–1331.
38. Yki-Järvinen H, Young AA, Lamkin C, Foley JE. Kinetics of glucose disposal in whole body and across the forearm in man. *J Clin Invest*. 1987;79(6):1713–1719.
39. Kotronen A, et al. A common variant in PNPLA3, which encodes adiponutrin, is associated with liver fat content in humans. *Diabetologia*. 2009;52(6):1056–1060.
40. Gastaldelli A, Coggan AR, Wolfe RR. Assessment of methods for improving tracer estimation of non-steady-state rate of appearance. *J Appl Physiol*. 1999;87(5):1813–1822.
41. Robinson MD, Oshlack A. A scaling normalization method for differential expression analysis of RNA-seq data. *Genome Biol*. 2010;11(3):R25.
42. Robinson MD, McCarthy DJ, Smyth GK. edgeR: a Bioconductor package for differential expression analysis of digital gene expression data. *Bioinformatics*. 2010;26(1):139–140.
43. Leek JT. svaseq: removing batch effects and other unwanted noise from sequencing data. *Nucleic Acids Res*. 2014;42(21):10.1093/nar/gku864.
44. Law CW, Chen Y, Shi W, Smyth GK. voom: Precision weights unlock linear model analysis tools for RNA-seq read counts. *Genome Biol*. 2014;15(2):R29.
45. Ritchie ME, et al. limma powers differential expression analyses for RNA-sequencing and microarray studies. *Nucleic Acids Res*. 2015;43(7):e47.
46. Phipson B, Lee S, Majewski IJ, Alexander WS, Smyth GK. Robust hyperparameter estimation protects against hypervariable genes and improves power to detect differential expression. *Ann Appl Stat*. 2016;10(2):946–963.
47. Yu G. enrichplot: Visualization of Functional Enrichment Result. Bioconductor. https://bioconductor.org/packages/release/bioc/html/enrichplot.html. Accessed March 2, 2020.
48. Yu G, Wang LG, Han Y, He QY. clusterProfiler: an R package for comparing biological themes among gene clusters. *OMICS*. 2012;16(5):284–287.
49. Storey JD, Bass AJ, Dabney A, Robinson D. qvalue: Q-value estimation for false discovery rate control. https://www.bioconductor.org/packages/release/bioc/html/qvalue.html. Accessed March 2, 2020.